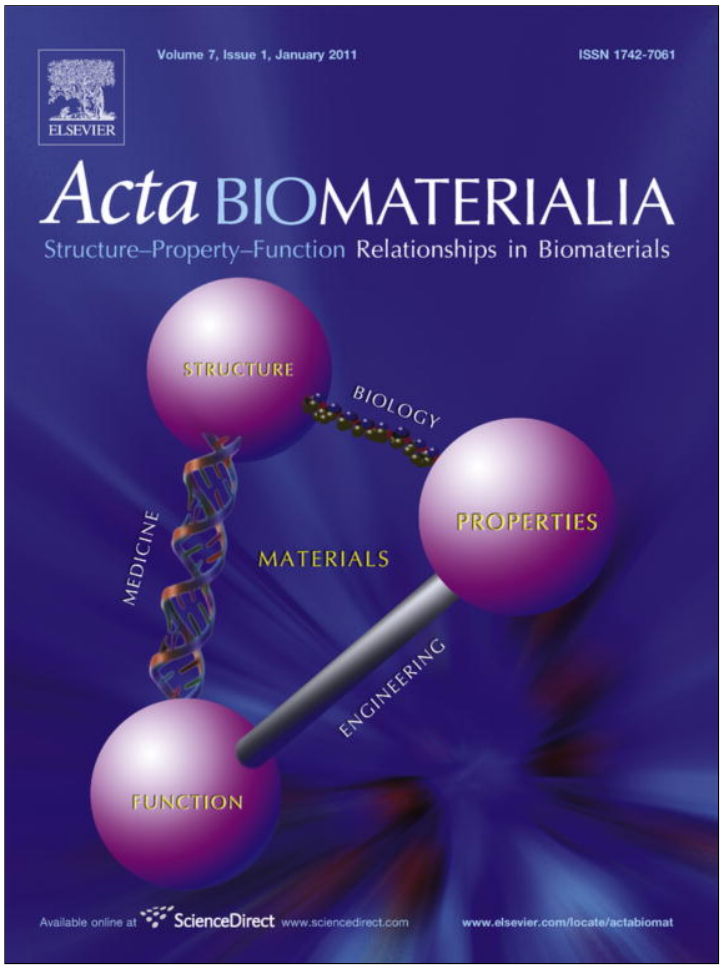

Acta Biomaterialia 7 (2011) 57–66

Contents lists available at ScienceDirect

Acta Biomaterialia

journal homepage: www.elsevier.com/locate/actabiomat

Mechano-topographic modulation of stem cell nuclear shape on nanofibrous scaffolds

Ashwin S. Nathan [a,b], Brendon M. Baker [a,b], Nandan L. Nerurkar [a,c], Robert L. Mauck [a,b,*]

[a] McKay Orthopaedic Research Laboratory, Department of Orthopaedic Surgery, University of Pennsylvania, Philadelphia, PA 19104, USA
[b] Department of Bioengineering, University of Pennsylvania, Philadelphia, PA 19104, USA
[c] Department of Mechanical Engineering and Applied Mechanics, University of Pennsylvania, Philadelphia, PA 19104, USA

ARTICLE INFO

Article history:
Received 4 June 2010
Received in revised form 19 July 2010
Accepted 9 August 2010
Available online 13 August 2010

Keywords:
Mesenchymal stem cells
Nanofibers
Nuclear orientation
Anisotropy
Cytoskeleton

ABSTRACT

Stem cells transit along a variety of lineage-specific routes towards differentiated phenotypes. These fate decisions are dependent not just on the soluble chemical cues that are encountered or enforced in vivo and in vitro, but also on physical cues from the cellular microenvironment. These physical cues can consist of both nano- and micro-scale topographical features, as well as mechanical inputs provided passively (from the base properties of the materials to which they adhere) or actively (from extrinsic applied mechanical deformations). A suitable tool to investigate the coordination of these cues lies in nanofibrous scaffolds, which can both dictate cellular and cytoskeletal orientation and facilitate mechanical perturbation of seeded cells. Here, we demonstrate a coordinated influence of scaffold architecture (aligned vs. randomly organized fibers) and tensile deformation on nuclear shape and orientation. Sensitivity of nuclear morphology to scaffold architecture was more pronounced in stem cell populations than in terminally differentiated fibrochondrocytes. Tension applied to the scaffold elicited further alterations in nuclear morphology, greatest in stem cells, that were mediated by the filamentous actin cytoskeleton, but not the microtubule or intermediate filament network. Nuclear perturbations were time and direction dependent, suggesting that the modality and direction of loading influenced nuclear architecture. The present work may provide additional insight into the mechanisms by which the physical microenvironment influences cell fate decisions, and has specific application to the design of new materials for regenerative medicine applications with adult stem cells.

1. Introduction

Adult mesenchymal stem cells (MSCs) have generated considerable interest for regenerative medicine applications given their ready isolation for autologous use, their extensive in vitro expansion capacity and their ability to differentiate along a number of different tissue-specific lineages, particularly those of the musculoskeletal system [1]. Most notably, adult MSCs appropriately cultured and provided with key soluble factors can adopt differentiated functions consistent with those of chondrocytes, adipocytes, and osteocytes [2,3]. Since this first conception of an adult stem cell it has been noted that additional cues from the microenvironment, including both passive (topography, order and substrate stiffness) and dynamic mechanical inputs can further regulate these phenotypic shifts [4,5].

These microenvironmental cues are particularly important for tissue engineering, where stem cells must often interface with a biomaterial substrate that can instruct tissue formation or serve as a vehicle for targeted delivery of cells in vivo. Design of the material microenvironment, for example through engineering specific receptor–ligand interactions on the material surface, can modulate the extent to which differentiation occurs [6,7]. Similarly, the topography of the interacting surface can be altered so as to have an impact on stem cell fate, whether these cells are delivered with or invade the biomaterial post-implantation [8,9]. While the mechanism by which these passive topographical stimuli elicit changes in stem cell activity is not yet clear, their influence occurs over a range of length scales and appears to influence the differentiation process directly.

Nanofibrous scaffolds formed by electrospinning are commonly employed for tissue engineering with stem cells [10]. These scaffolds provide a biomimetic fibrous microenvironment with polymeric fibers that recreate the length scale encountered by cells within their normal extracellular milieu. Adult MSCs seeded onto these scaffolds can differentiate along multiple lineages [11] Nanofibrous scaffolds, by virtue of their nano-scale features, also

* Corresponding author at: McKay Orthopaedic Research Laboratory, Department of Orthopaedic Surgery, University of Pennsylvania, Philadelphia, PA 19104, USA. Tel.: +1 215 898 3294; fax: +1 215 573 2133.
E-mail address: lemauck@mail.med.upenn.edu (R.L. Mauck).

1742-7061/$ - see front matter © 2010 Acta Materialia Inc. Published by Elsevier Ltd. All rights reserved.
doi:10.1016/j.actbio.2010.08.007

influence cell shape and, therefore, biological responses directly. For example, primary chondrocytes on nanofibrous scaffolds produce higher levels of cartilage-specific matrix compared with the same cells seeded on micron-scale fibers of the same composition [12]. Nanofibrillar surfaces also control mouse embryonic fibroblast morphology and cytoskeletal organization [13], enhance proliferation and self-renewal of mouse embryonic stem cells [14] and activate cytoskeletal remodeling through the small GTPase Rac [15]. We have recently shown that the alignment of this nanofibrous microenvironment can direct actin stress fiber organization in adult human MSCs [16]. This, in turn, directs the ordered deposition of the matrix, which in the long-term, translates to improved construct mechanical properties [17,18]. Of particular note, and in comparison with traditional pellet culture, the aligned topography provided by these organized nanofibrous patterns can foster fibrous over cartilaginous differentiation of MSCs [19].

In addition to these passive cues provided by the material microenvironment, active mechanical cues likewise exert control over stem cell differentiation. Physical forces applied to MSCs in vitro, often carried out via deformation of scaffolds with custom mechanical devices [20,21], can increase collagen gene expression by MSCs after one day [22], and improve osteogenesis and mineral deposition over several days [23]. On dynamically loaded unpatterned surfaces most cells reorient such that their long axis is perpendicular to the prevailing strain direction [24,25]. To force cells to adopt a specific morphology with respect to the applied strain, constraints have been applied via aligned microgrooves on elastomeric subtractes produced by soft lithography [24,26]. Using such methods, Kurpinski and co-workers showed that with dynamic tensile deformation applied in the microgroove direction, MSCs increased both proliferation and smooth muscle marker gene expression, while chondrogenic matrix marker expression decreased [27]. Interestingly, when strain was applied perpendicular to the cell axis, a different set of genes was activated and proliferation rates were no longer altered, suggesting that mechanosensing by MSCs is anisotropic (direction dependent).

Cells are inextricably linked to their extracellular environment via complex interpenetrating cytoskeletal networks [28,29]. These networks provide a rapid and efficient means by which extracellular and intracellular perturbations can be transmitted to cell structures such as the nucleus [30–32]. Nuclear shape and deformation in turn correlate with gene expression changes. For example, when pre-osteoblast cells are confined to specific micropatterned geometries, an ideal ratio of nuclear area to height promotes collagen gene expression [33]. In tissues and tissue-like engineered constructs, nuclear deformation is associated with changes in cellular biosynthetic activities [34,35]. In chondrocytes, de-differentiation in monolayer culture is associated with an increase in nuclear spreading as the cells flatten. Recovery of a round nucleus with cytochalasin D treatment restores cartilage-specific gene expression [36]. Likewise, disruption of actin networks in embryoid body-derived cells promotes the chondrogenic phenotype [37]. Furthermore, the mechanical properties of the embryonic cell nucleus change as a function of differentiation status [38,39], raising the intriguing possibility that physical cues (active and passive) will be interpreted differently by the same cell, depending on which lineage is adopted and how far along that lineage specification the cell has proceeded.

To begin addressing these questions in the context of nanofibrous scaffolds, here we have investigated the impact of scaffold fiber organization and deformation on nuclear morphology in both adult human MSCs and differentiated fibrochondrocytes from the knee meniscus. We hypothesized that the degree of order within the extracellular microenvironment would provide a 'set point' for nuclear morphology, and that mechanical perturbation of the fibrous network would elicit further changes via nuclear realignment and deformation. We further queried the role of cytoskeletal elements in defining the baseline nuclear shape and transmitting external loads to the nucleus as a function of both time and loading direction. Our findings demonstrate an increased sensitivity of undifferentiated cells to the alignment of the nanofibrillar matrix and implicate the actin cytoskeleton in transmission of exogenous forces.

2. Materials and methods

2.1. Scaffold fabrication

Nanofibrous meshes were created using a custom electrospinning apparatus, as described previously [16,17]. Briefly, poly(ε-caprolactone) (PCL) (80 kDa, Sigma-Aldrich, St Louis, MO) was dissolved to 14.3% w/v in a 1:1 solution of tetrahydrofuran and *N*,*N*-dimethylformamide (Fisher Chemical, Fairlawn, NJ). The solution was ejected from the spinneret at 2.5 ml h^{-1} via a syringe pump through an 18G stainless steel blunt-ended needle charged to +13 kV with a high voltage power supply (ES30N-5W, Gamma High Voltage Research, Ormond Beach, FL). Fibers were collected on a grounded mandrel over an air gap of 15 cm. To create non-aligned (NA) meshes lacking a preferred fiber direction the mandrel was rotated slowly throughout the collection process (surface velocity 0.5 m s^{-1}). To form scaffolds with aligned (AL) nanofibers the surface velocity was increased to 17.5 m s^{-1} [16]. Fibers were collected for 4 h to produce mats of ~0.7 mm thickness. 60 × 5 mm^2 strips were excised from the NA sheets in a random-orientation. AL samples of the same dimension were excised from fiber-aligned mats in either the predominant fiber direction or perpendicular to the fiber direction. To assess fiber organization, scaffolds were sputter coated with AuPd and visualized by scanning electron microscopy (SEM).

2.2. Cell isolation and seeding

Human MSCs and meniscal fibrochondrocytes were isolated from surgical waste tissue of three patients ranging in age from 51 to 63 years, who were undergoing total knee arthroplasty [40,41]. MSCs were isolated from tibial or femoral bone marrow aspirates via plastic adherence in basal medium (BM) (Dulbecco's minimal essential medium (DMEM) containing 1× penicillin/streptomycin/fungizone and 10% fetal bovine serum) as in Baker et al. [19]. Resected meniscus tissue was finely minced and plated in BM. Resident fibrochondrocytes migrated out of the tissue, and after 1 week the tissue fragments were removed. Adherent cells formed colonies and were subsequently expanded to passage 4 at a ratio of 1:3 in BM.

Prior to cell seeding nanofibrous strips were sterilized and rehydrated in decreasing concentrations of ethanol (100%, 70%, 50%, 30%) and soaked in a 20 μg ml^{-1} solution of human fibronectin for 16 h to promote cell attachment. For cell seeding each side of the scaffold received a 200 μl aliquot containing 60 × 10^4 cells (either MSCs or fibrochondrocytes), followed by 2 h incubation to allow for attachment. Cell seeded scaffolds were maintained in a chemically defined medium [42] (CDM) (high glucose DMEM with 1× penicillin/streptomycin/fungizone, 0.1 μM dexamethasone, 50 μg ml^{-1} ascorbate 2-phosphate, 40 μg ml^{-1} L-proline, 100 μg ml^{-1} sodium pyruvate, 6.25 μg ml^{-1} insulin, 6.25 μg ml^{-1} transferrin, 6.25 ng ml^{-1} selenous acid, 1.25 mg ml^{-1} bovine serum albumin and 5.35 μg ml^{-1} linoleic acid) for 16 h prior to experimentation. Where indicated, media were further supplemented with 2.0 mM acrylamide (ACR) (National Diagnostics, Atlanta, GA), 1.7 μM nocodazole (NOC) (Sigma–Aldrich, St. Louis, MO) or 1 nM cytochalasin D (CYD) (Sigma–Aldrich, St. Louis, MO) to disrupt intermediate filaments, microtubules and actin filaments, respectively [43,44].

These values represent the minimum concentration that visibly disrupted the element without altering normal cell morphology (see below).

2.3. Mechanical loading

A custom tensile stretching device was developed to apply precise static deformations to cell seeded nanofibrous scaffolds on the stage of an inverted fluorescent microscope (Fig. 1A and B). The device consisted of a linear stage fitted with a manual actuator/micrometer (Newport, Irvine, CA), two anodized aluminum braces and removable polysulfone grips. To determine the relationship between the deformations applied with the device and surface strain on the scaffold, acellular aligned PCL strips were speckle coated with black enamel [45] and mounted in the device. Tensile deformations of up to 10% grip-to-grip strain were applied in 2.5% increments with 1 min rest between steps; images were acquired before and after each step using a digital camera (A1021, Basler, Ahrensburg, Germany). Scaffold stress–relaxation behavior was characterized using an Instron 5542 mechanical test system (Instron, Canton, MA). Speckled samples were preloaded to 0.1 N, ramped to 10% of the gauge length at 0.1% s^{-1} and held for 2 h. Texture correlation analysis of local deformation was performed on the central third of each scaffold using Vic2D (Correlated Solutions, Columbia, SC) as in Nerurkar et al. [45].

To image cell and nuclear deformation, cell seeded constructs were fitted into the tensile loading device and extended to 0, 5 or 10% grip-to-grip strain at 0.1% s^{-1}. Constructs were either fixed immediately in 4% paraformaldehyde or were cultured at 37 °C in CDM for an extended duration in the stretched state (5, 15 or 30 min or 1 or 2 h) prior to fixation. All samples were fixed, stained and imaged within the custom tensile device in the deformed state. To examine cytoskeletal elements, cells were permeabilized with Triton X-100 and stained with either anti-vimentin (Millipore, Billerica, MA) to visualize intermediate filaments, anti-α-tubulin mAb–Alexa488 (Invitrogen, Carlsbad, CA) to visualize microtubules or phalloidin–Alexa488 (Invitrogen, Carlsbad, CA) to visualize actin, according to the manufacturer's instructions. Nuclei were labeled with 4′,6-diamidino-2-phenylindole (DAPI). Images were obtained on a Nikon T30 inverted fluorescent microscope equipped with a CCD camera (Nikon Instruments, Melville, NY).

2.4. Quantification of nuclear morphology

To quantify the nuclear aspect ratio (NAR) and the orientation angle of the nucleus, a custom code was developed in MATLAB (The Mathworks, Natick, MA). Briefly, grayscale images of DAPI-stained nuclei were thresholded and each nucleus was assigned a cluster identity. Each cluster of pixels representing a nucleus was subjected to principal component analysis in order to determine its long and short axis and orientation. The NAR was defined as the ratio of the long axis to the short axis and the orientation angle was defined as the angle between the long axis of the nucleus and the direction of loading (Fig. 2C).

2.5. Statistical analysis

Analysis of variance was performed using the statistical software package SYSTAT v. 10.2 (Point Richmond, CA) with Bonferroni post-hoc tests used to make pair-wise comparisons. Significance

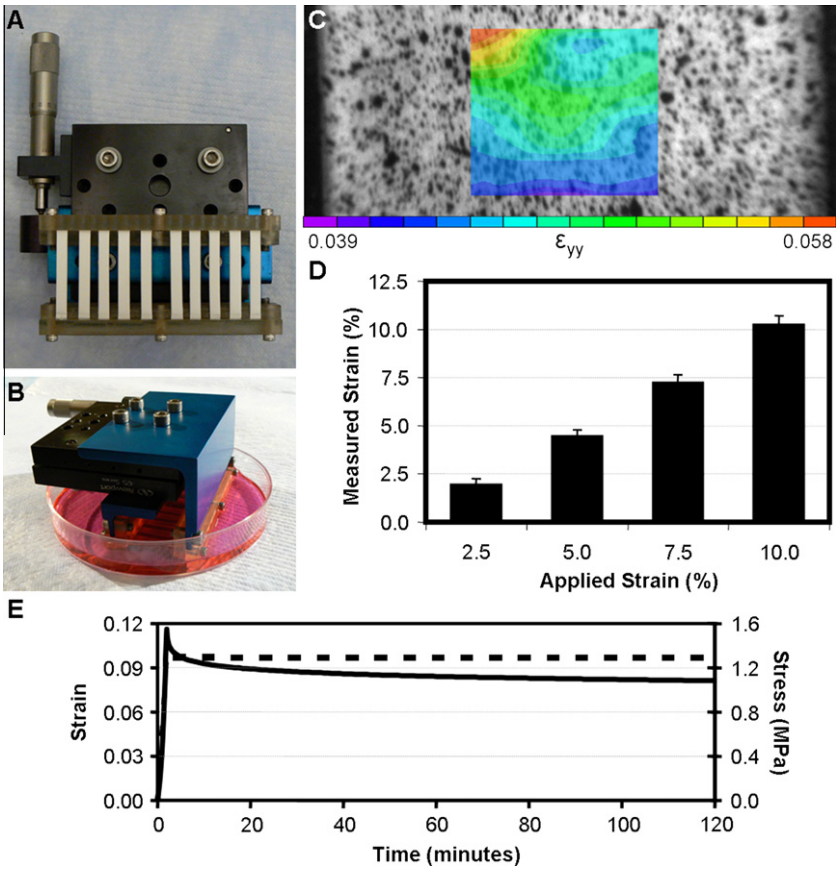

Fig. 1. Construction and validation of a custom system for applying controlled tensile deformation to cell seeded nanofibrous scaffolds. (A and B) Custom device for applying tension to constructs in vitro. (C) Texture correlation of a speckled scaffold under 5% applied strain reveals relatively homogeneous surface strains. (D) Average surface strains correlate well with applied strain ($n = 6$). (E) Representative stress (solid line) and strain (dashed line) responses of an aligned nanofibrous scaffold held at 10% strain for 2 h.

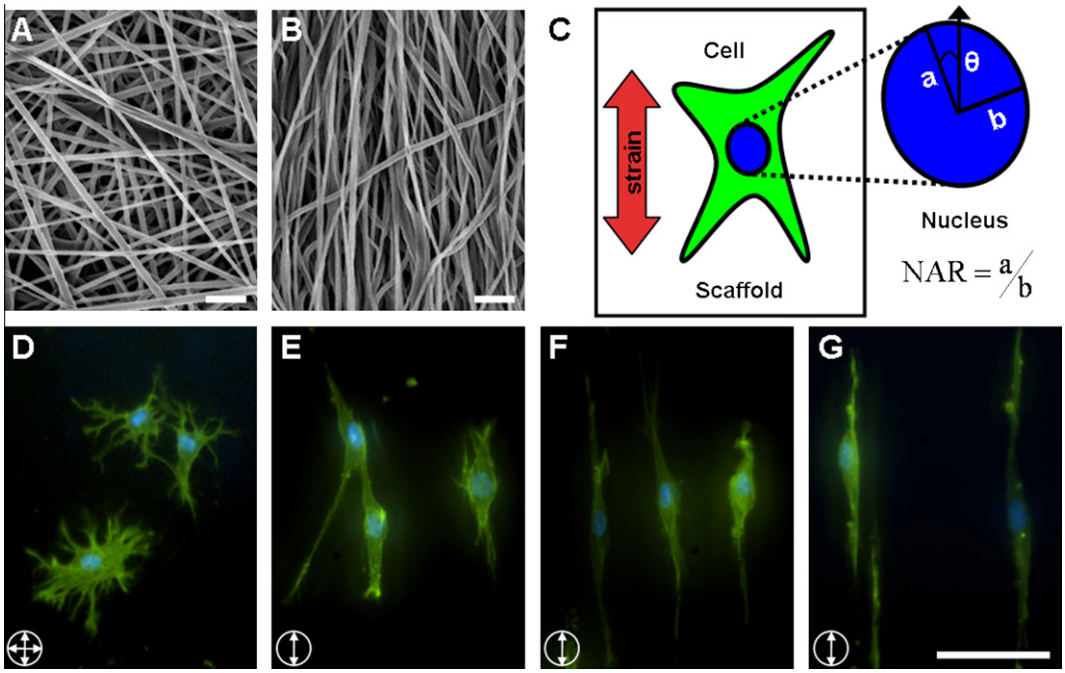

Fig. 2. The organization of nanofibers dictates the initial morphology of seeded cells. SEM images of (A) non-aligned and (B) aligned PCL nanofibers (scale bar 10 μm). (C) To quantify sub-cellular morphological changes, the nuclear aspect ratio (NAR) and orientation angle (θ) were quantified. The NAR was defined as the ratio of the long axis (a) to the short axis (b) of the nucleus and θ was defined as the angle between the long axis (a) and the direction of stretch. Representative images of meniscal fibrochondrocytes seeded on (D) NA and (E) AL nanofibrous scaffolds and AL constructs deformed to (F) 5% and (G) 10% strain (scale bar 20 μm). Cells were fluorescently labeled for F-actin (green) and DNA (blue).

was set at $P \leqslant 0.05$. For both MSCs and fibrochondrocytes, the entire experiment was performed in duplicate, with differences due to cell type, scaffold deformation and nanofiber alignment remaining consistent across replicates. Within each donor replicate, more than 500 cells per condition were quantified on at least three distinct scaffolds and were pooled for analysis for each scaffold and cell type, time point and strain level. Representative experiments are shown, with all data presented as means ± standard deviation.

3. Results

3.1. Mechanical response of nanofibrous scaffolds to static tensile deformation

A system for applying static tensile deformation to nanofibrous scaffolds was designed and validated (Fig. 1A and B). To ensure that local strains were macroscopically homogeneous and consistent with the applied strain, the relationship between applied and surface strain was determined using texture correlation. At all levels of applied strain, the region of interest (central third) had a relatively homogeneous strain distribution (Fig. 1C). Applied strain also correlated well with average surface strain (Fig. 1D, $R^2 = 0.997$, $P < 0.001$), with a slope of 1.15. As some studies of cellular function were conducted over the course of several hours, the time varying mechanical behavior of nanofibrous scaffolds under static deformation was assessed. Scaffolds were extended by 10% of their initial length and held for 2 h (Fig. 1E). The stress peaked with the applied strain and relaxed by ~30% over the ensuing 2 h, with the greatest decrease in stress occurring in the first 3 min. Surface strains determined by texture correlation remained constant over the 2 h period at 10%.

3.2. Translation of topographical and mechanical cues to nuclear deformation

SEM imaging of electrospun scaffolds confirmed the formation of randomly oriented non-aligned (Fig. 2A) and highly aligned scaffold topographies (Fig. 2B). Cells seeded onto these distinct architectures adopted morphologies that reflected the underlying fiber topography. Cells on non-aligned scaffolds were well spread, with actin-rich processes extending isotropically (Fig. 2D). In contrast, cells on aligned scaffolds had fewer and larger processes, extending exclusively along the fiber direction (Fig. 2E). While results are shown only for fibrochondroctyes (Fig. 2D and E), MSCs behaved similarly, as has been shown previously [19].

The pronounced effect of scaffold architecture on cell morphology translated to quantifiable differences in nuclear geometry and organization. Changes in nuclear shape were quantified by measurement of the nuclear aspect ratio (NAR) by normalizing the lengths of the long to short axes (Fig. 2C). In monolayer culture on tissue culture plastic and on non-aligned nanofibrous scaffolds, the nuclei of MSCs were elliptical, possessing a NAR of ~1.5 (Fig. 3A). When the same cells were seeded on aligned scaffolds, the nuclei became more elongated in the fiber direction, increasing the NAR to ~1.7 ($P < 0.001$). Compared with MSCs, fibrochondrocytes began with a lower NAR on non-aligned scaffolds (1.34 ± 0.30 vs. 1.52 ± 0.49) and increased on aligned scaffolds, albeit to a much lesser extent than MSCs (1.41 ± 0.32 vs. 1.71 ± 0.44) (Fig. 3B). The angle between the direction of fiber alignment and the principal orientation of the nucleus was determined and binned into angular histograms (Fig. 3C and D). As expected, the distribution of nuclear orientation on non-aligned scaffolds was random, with a mean angle of ~45° (Fig. 3C). In contrast, cell nuclei on aligned scaffolds were parallel to the fiber direction (Fig. 3D). For both cell types, the majority of nuclei were aligned within ±25° of the predominant fiber direction, with a mean angle of 21° and 24° for MSCs and fibrochondrocytes, respectively.

Next, constructs were elongated by 5% or 10% of their initial length and immediately fixed to determine how deformation of the nanofibrous scaffold translated to cell and nuclear deformation. Both cell types, which were already highly polarized on aligned scaffolds, became further oriented and elongated with deformation along the direction of alignment (Fig. 2E–G). On non-aligned

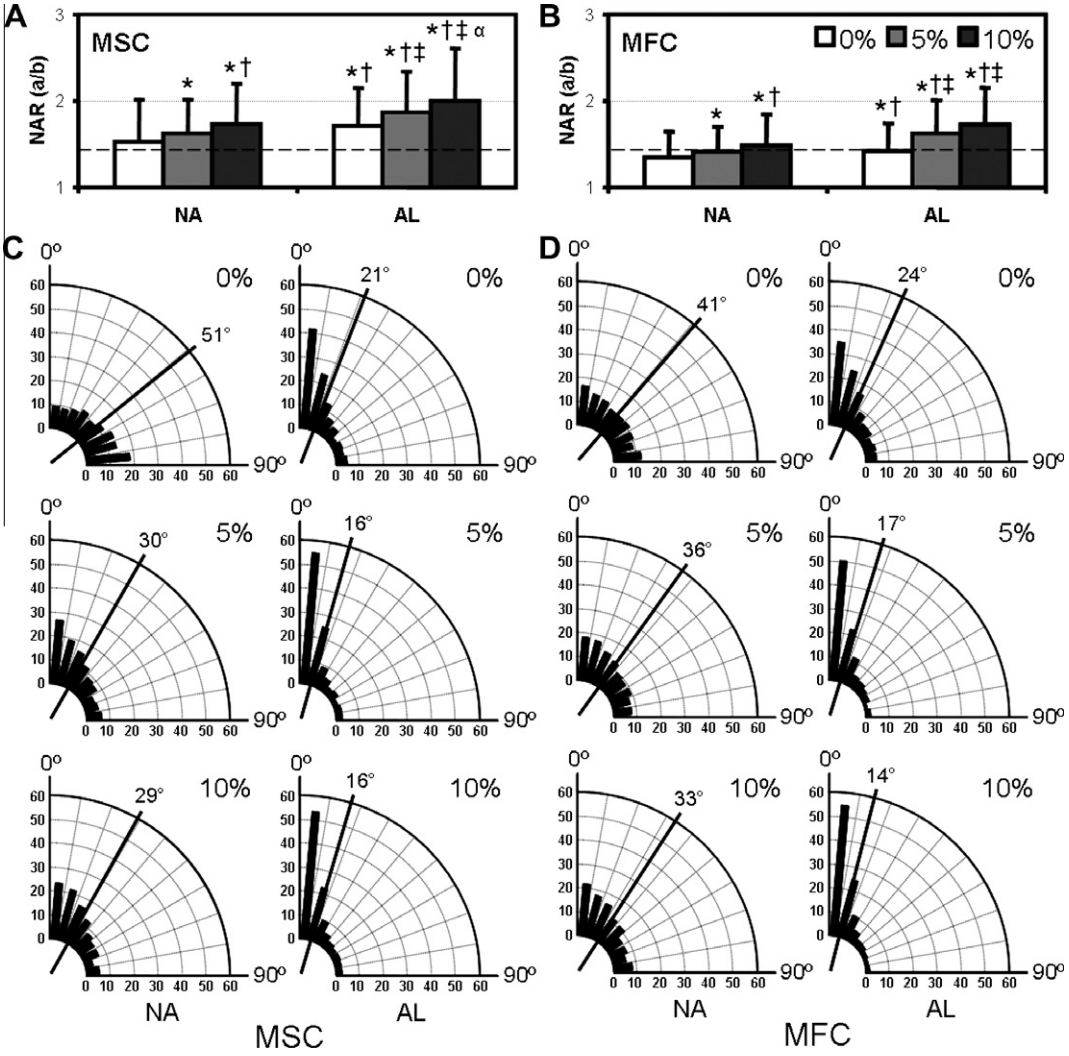

Fig. 3. Nuclear morphology and orientation are dependent upon scaffold architecture and applied strain. NAR of (A) MSC and (B) fibrochondrocyte (MFC) seeded NA and AL scaffolds with increasing levels of applied strain ($n > 500$, $^{*}P < 0.05$ vs. 0% NA, $^{\dagger}P < 0.05$ vs. 5% NA, $^{\ddagger}P < 0.05$ vs. 0% AL, $^{\alpha}P < 0.05$ vs. 5% AL). Dashed lines indicate the NAR of the same cell populations cultured as monolayers. Angular histograms of the nuclear orientation of (C) MSC and (D) fibrochondrocyte NA and AL constructs at 0%, 5% and 10% strain. The radial axis indicates the percentage of the total cell population and the solid line represents the mean angle of the distribution.

scaffolds both cell types lengthened to a lesser extent (not shown). Consistent with these changes in cell morphology due to stretch, the nuclei of both cell types were sensitive to tensile deformation. On both non-aligned and aligned scaffolds, increasing levels of strain resulted in higher NARs, with this effect being more dramatic on aligned scaffolds. Furthermore, on both non-aligned and aligned scaffolds, tensile deformation induced nuclei to reorient in the direction of the applied load. For example, in MSC seeded non-aligned constructs a 10% deformation caused 30% more nuclei to align within ±20° with respect to the direction of loading, shifting the mean angle of the population from 51° to 29°. While trends were similar between the two cell types, the NAR of fibrochondrocytes were consistently lower than those of MSCs. Furthermore, the NAR did not increase from 5% to 10% strain in aligned fibrochondrocyte seeded constructs, suggesting that these differentiated cells had reached a maximum in nuclear deformation.

3.3. Temporal changes in NAR and orientation angle

While these experiments captured the instantaneous response of cells to mechanical perturbation of their underlying substrates, in some instances, cell and nuclear shape changes are transient when the mechanical stimulus is held constant [34]. To capture transient changes in nuclear deformation, fibrochondrocyte seeded aligned scaffolds were stretched to 10% strain and incubated for increasing durations of time prior to fixation and imaging. As above, 10% strain resulted in an immediate 30% increase in NAR relative to unstrained controls (Fig. 4A). However, when the deformation was held constant, the NAR decreased with time, despite no changes in scaffold deformation over this time course (Fig. 1E). Notably, the NAR dropped markedly over the first 5 min, before returning to baseline values at a more gradual rate. After 2 h the NAR of cells on constructs strained to 10% were not different from unstrained controls ($P = 0.475$).

Paralleling these temporal changes in NAR, nuclear orientation also relaxed during continuously applied static deformation (Fig. 4B). Prior to strain, a large population of nuclei were already polarized as a consequence of the aligned fiber topography, translating to a mean angle of 19°. The application of 10% strain further oriented the population in the direction of the load, as evidenced by an increase in the fraction of cells in the ±10° bin and a mean angle of 11°. As the NAR decreased over the first 15 min, the nuclei also began to relax towards a wider distribution of orientation angles. The mean angle increased to 15° and the angular histogram

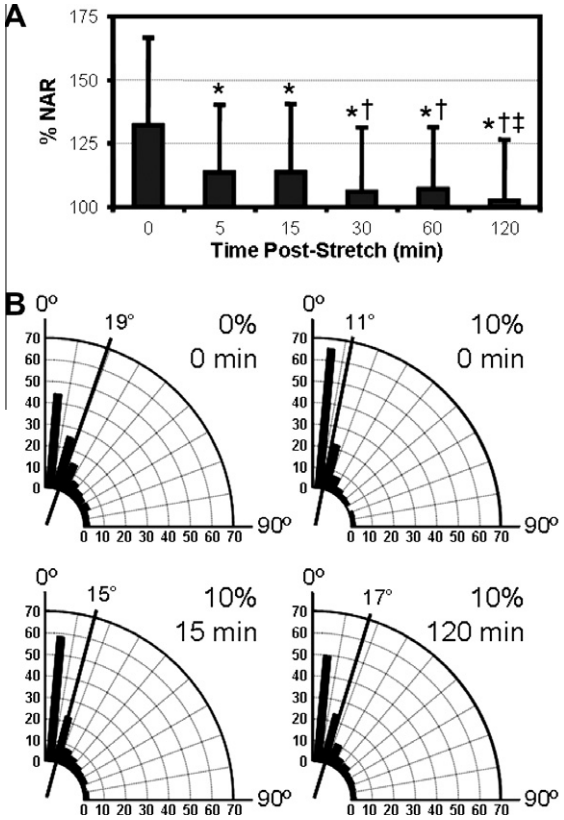

Fig. 4. Time-dependent nuclear relaxation with static scaffold deformation. (A) The percentage change in NAR (relative to undeformed values) of fibrochondrocyte seeded constructs at increasing time intervals after application of 10% strain ($n > 500$, $^{*}P < 0.05$ vs. 0 min, $^{\dagger}P < 0.05$ vs. 15 min, $^{\ddagger}P < 0.05$ vs. 60 min). (B) Angular histograms of nuclear orientation prior to stretch, immediately after stretch and after 15 or 120 min ($n > 500$).

revealed a profile intermediate between the pre- and post-strain states. By 120 min, the angular profile and mean angle of the population closely mimicked the undeformed scenario.

3.4. Cytoskeletal mediation of nuclear changes

As demonstrated in the above studies, a deformation of the nanofibrous substrate was transduced through the cell to dynamic changes in the geometry and alignment of the nucleus. To investigate the role of the cytoskeleton in this nuclear deformation, actin microfilaments, microtubules and intermediate filaments were perturbed. Fluorescent staining confirmed the presence of these sub-cellular structures in both MSCs and fibrochondrocytes on nanofibrous scaffolds. Microtubules radiated outward from the center of the cell and were highly aligned with the cell body (and direction of nanofiber alignment) (Fig. 5A). Vimentin, an intermediate filament protein, did not span the entire cytoplasm, but rather was concentrated around the nucleus (Fig. 5B). Actin was present throughout the cytoplasm, forming dense stress fibers that were aligned with the long axis of the cell (Fig. 5C).

To identify the cytoskeletal element responsible for the observed increase in NAR with scaffold deformation, microtubules, intermediate filaments and filamentous actin were depolymerized with NOC, ACR and CYD, respectively (Fig. 5D–F). In the presence of chemical inhibitors, the filamentous form of these biopolymers became less prevalent: microtubules became tightly localized to the nucleus, intermediate filament staining diminished in intensity and was completely absent in some cells, and actin stress fibers were reduced to short microfilaments visible as punctate staining. Disruption of the microtubule and intermediate filament networks did not influence the actin cytoskeleton or overall cell morphology (Fig. 4G and H).

Next, the change in NAR with 10% strain was examined in nanofibrous constructs cultured in the presence of these cytoskeletal disruptors. The baseline NAR of aligned MSCs in control medium prior to the application of strain was 1.7 (CTRL, Fig. 6A). As before, 10% applied strain increased this value to 2.0. The same effect of strain was observed despite the disruption of microtubules and intermediate filaments (NOC and ACR, Fig. 6A). However, the removal of actin completely abrogated this response, with no change in NAR with scaffold deformation (CYD, Fig. 6A). These same trends held for fibrochondrocyte seeded constructs (Fig. 6B). Interestingly, in the absence of applied strain, NAR increased significantly in MSCs whose microtubules and intermediate filaments were disrupted, a behavior that was not observed in fibrochondrocytes treated similarly (Fig. 6).

3.5. Directional control of NAR and orientation angle

To further elucidate the interplay between scaffold topography and loading direction, cells on aligned nanofibrous scaffolds were stretched either parallel (||) or perpendicular ($\perp$) to the fiber direction (Fig. 7A). As in previous experiments, strain applied in the direction of the fibers increased the NAR and induced further alignment of the nuclei (|| CTRL, Fig. 7B and D). Conversely, strain applied transverse to the fibers resulted in a minor but significant decrease in NAR, indicating that nuclei became rounder in shape ($\perp$ CTRL, Fig. 7B). Examining the magnitude rather than direction of change, an identical 10% strain applied parallel or perpendicular to the fiber direction resulted in a 32% or 7% change in NAR, respectively. In contrast to parallel strains, angular histograms did not reveal marked reorientation of nuclei under perpendicular loading ($\perp$ CTRL, Fig. 7D). In the presence of CYD the strain-induced changes in NAR in either the parallel or perpendicular directions were abrogated (|| or $\perp$ CYD, Fig. 7B). Disruption of the actin cytoskeleton also prevented nuclei from reorienting with scaffold deformation in either direction, confirming the role of actin in not only transmitting mechanical forces to the nucleus, but also in dictating nuclear reorientation (Fig. 7D). Further to these changes in NAR, the projected nuclear area was altered with respect to deformation. With parallel strain, the nuclear area decreased, while in the presence of CYD no such response was evoked. With perpendicular strain, there was a small but significant increase in area under both control and CYD conditions.

4. Discussion

A variety of cues presented by or transmitted through the cellular microenvironment regulate stem cell fate decisions. Conventionally, the nucleus is considered the center wherein soluble second messengers arising from external physical and chemical signals are integrated to direct an overall cell response. While the mechanisms by which nuclear geometry, mechanics, and deformation have an impact on cell function and signaling are not yet clear, it is now understood that mRNA diffusion through the nucleus changes based on local chromosomal density [46] and that marked alterations in chromosomal territory location occur with specification of cell fate [47]. External cues (passive or active) that alter nuclear shape may thus change the integration and transmission of signals. Indeed, recent work suggests that the resting shape and deformation of the nucleus itself directly alters transcriptional events [32] and precise control of nuclear shape via controlled microprinted templates regulates collagen expression in osteo-progenitor cells [33]. Our work with nanofibrous networks suggests that this nano-scale topography likewise alters

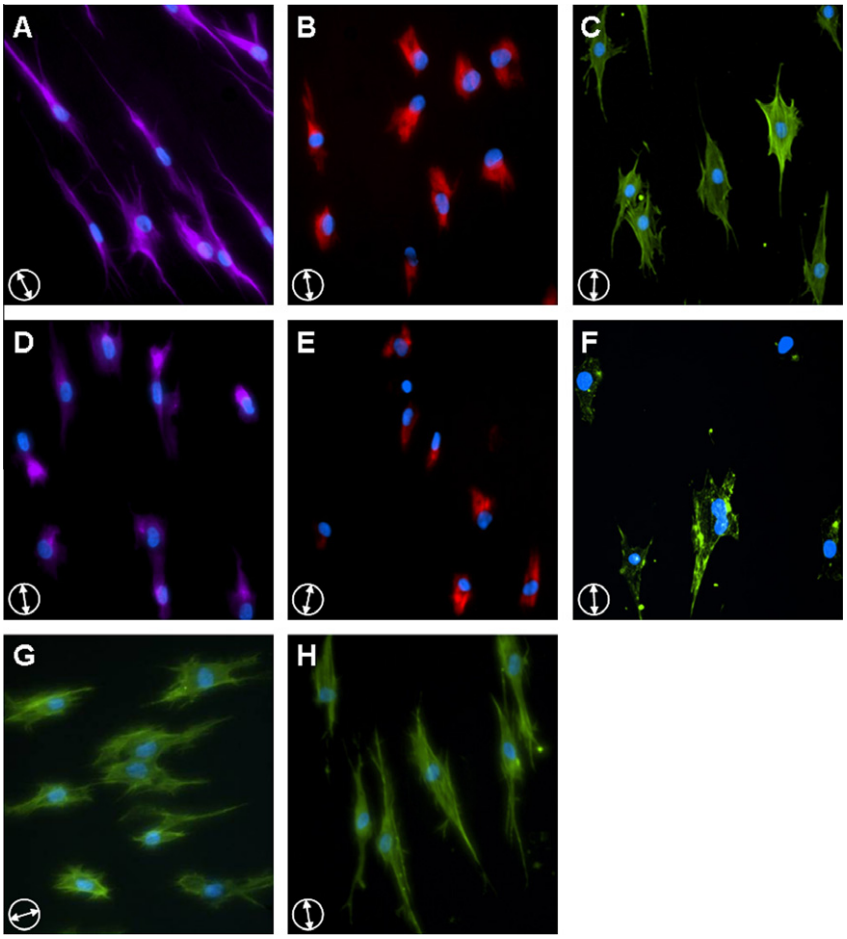

Fig. 5. Selective disruption of cytoskeletal elements does not alter cell morphology on nanofibrous scaffolds. Fibrochondrocytes on AL scaffolds stained for (A) microtubules (purple), (B) intermediate filaments (red) and (C) F-actin (green). Constructs were exposed to (D) nocodazole, (E) acrylamide and (F) cytochalasin D to disrupt microtubule, intermediate filament and F-actin networks, respectively. Additional samples were treated with (G) nocodazole or (H) acrylamide and stained with phalloidin to confirm that the removal of these elements did not alter the actin cytoskeleton. All images were counterstained for cell nuclei (blue). Scale bar 20 μm, arrows denote nanofiber direction.

cellular activity. For example, MSCs seeded on aligned scaffolds reduce chondrogenic and increase fibrous marker expression compared with traditional pellet cultures [19]. Moreover, dynamic tensile loading applied over long time periods increases expression of these same fibrous markers, and ultimately leads to more matrix production and enhanced mechanical function in engineered constructs [48]. Based on these findings, the present study investigated how nuclear morphology is defined by nanofibrous networks of differing organization and how this morphology changed when scaffolds were subjected to tensile deformation.

In this study, we have evaluated how the nuclei of two cell types, MSCs and fibrochondrocytes, respond to the presentation of differing nanofibrous topographies. These two cell types were chosen to represent an uncommitted progenitor cell population (MSCs) and a mature, differentiated cell population (fibrochondrocytes from the meniscus). Evaluation of NARs showed that simply presenting these cells with a nanofibrous topography altered nuclear shape – MSC nuclei on aligned scaffolds were more elongated (i.e. had a higher NAR) than on either non-aligned scaffolds or on tissue culture plastic. Notably, NAR for the differentiated fibrochondrocyte population changed only slightly with changing topography. It has recently been suggested that the quantity and quality of the MSC cytoskeleton (and so cell mechanical properties) are altered by substrate topography. Lim and co-workers showed that MSCs are softer and contain less actin on nano-patterned tissue culture plastic (500 nm gratings) compared with flat plastic [49]. In our work, fibrochondrocytes and MSCs were indistinguishable from one another on either aligned or non-aligned scaffolds in the undeformed state, containing dense actin networks with clearly visible stress fibers [16,19]. As the cytoskeletal network is similar in both cell types, the observed difference in NAR under load may alternatively reflect changes in nuclear stiffness. While the nucleus is generally considered the stiffest element within the cell [50], the intrinsic stiffness of the nucleus increases with differentiation, potentially due to changes in nuclear envelope protein type and amount [39]. Thus, the different nuclear morphology observed for MSCs compared with fibrochondrocytes may reflect the changing mechanical properties of the nucleus relative to the cytoskeletal network in which it is ensconced. Future studies will further query this possibility through direct mechanical testing of the MSC nucleus as cells undergo fibrochondrogenesis.

To investigate how exogenous deformation, superimposed on these base topographies, might further modulate nuclear shape we developed a custom tensile loading device and validated transfer of strain to the scaffold surface. Increasing tensile deformation led to increases in NAR for each cell type. At each step (5% and 10%) NAR increased significantly for MSCs on both non-aligned and aligned scaffolds. Conversely, a significant increase was observed only for the first 5% strain step for fibrochondrocytes on aligned scaffolds. This may reflect a limit on nuclear deformation in these differentiated cells, potentially related to the maturity of the nuclear lamina [51]. Overall, the findings above are consistent with

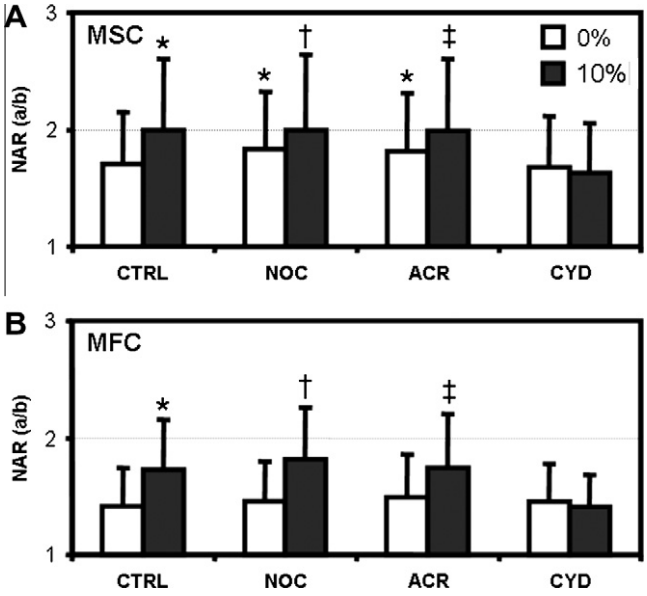

Fig. 6. Disruption of the actin cytoskeleton abrogates strain-induced alterations in NAR. (A) MSC and (B) fibrochondrocyte (MFC) seeded constructs were cultured in either control medium (CTRL) or the same medium supplemented with nocodazole (NOC), acrylamide (ACR) or cytochalasin D (CYD) prior to application of 10% strain ($n > 500$, $^{*}P < 0.05$ vs. 0% CT, $^{\dagger}P < 0.05$ vs. 0% NO, $^{\ddagger}P < 0.05$ vs. 0% ACR). NAR was determined immediately after loading.

those reported by Stella and co-workers, who showed an increasing NAR in non-aligned polyurethane-based nanofibrous scaffolds seeded with vascular smooth muscle cells and subjected to biaxial tensile stretch [52]. In that study and the present one, nuclei were randomly oriented on non-aligned scaffolds, with a gradual alignment with the stretch direction with increasing deformation, suggestive of fiber reorientation with load. In the present study, however, nuclei on aligned scaffolds were already highly aligned after seeding, and showed the most marked increase in NAR between 0% and 5% strain. This would suggest that there was an immediate engagement of fibers on these aligned scaffolds, with only slight reorientation needed to align the cells with the loading direction.

When subjected to stretch and held in that configuration, NAR decayed to baseline levels with time, despite no time-dependent changes in the underlying scaffold. Indeed, the greatest decrease occurred over the first 5 min, with a steady decline to baseline levels over the next 2 h. This suggests, interestingly, that cells respond to static deformation by re-establishing their homeostatic nuclear configuration within minutes. Whether this return to baseline results from reorganization of the cytoskeleton that engendered the original perturbation in NAR or whether the relaxation was a purely viscoelastic phenomenon [50] is not yet known. For example, Putnam and co-workers showed a rapid increase in assembly of the microtubule network within 15 min of 10% static stretch of cells on an unpatterned elastomeric sheet [53]. Regardless of mechanism, these findings suggest temporal limitations of static

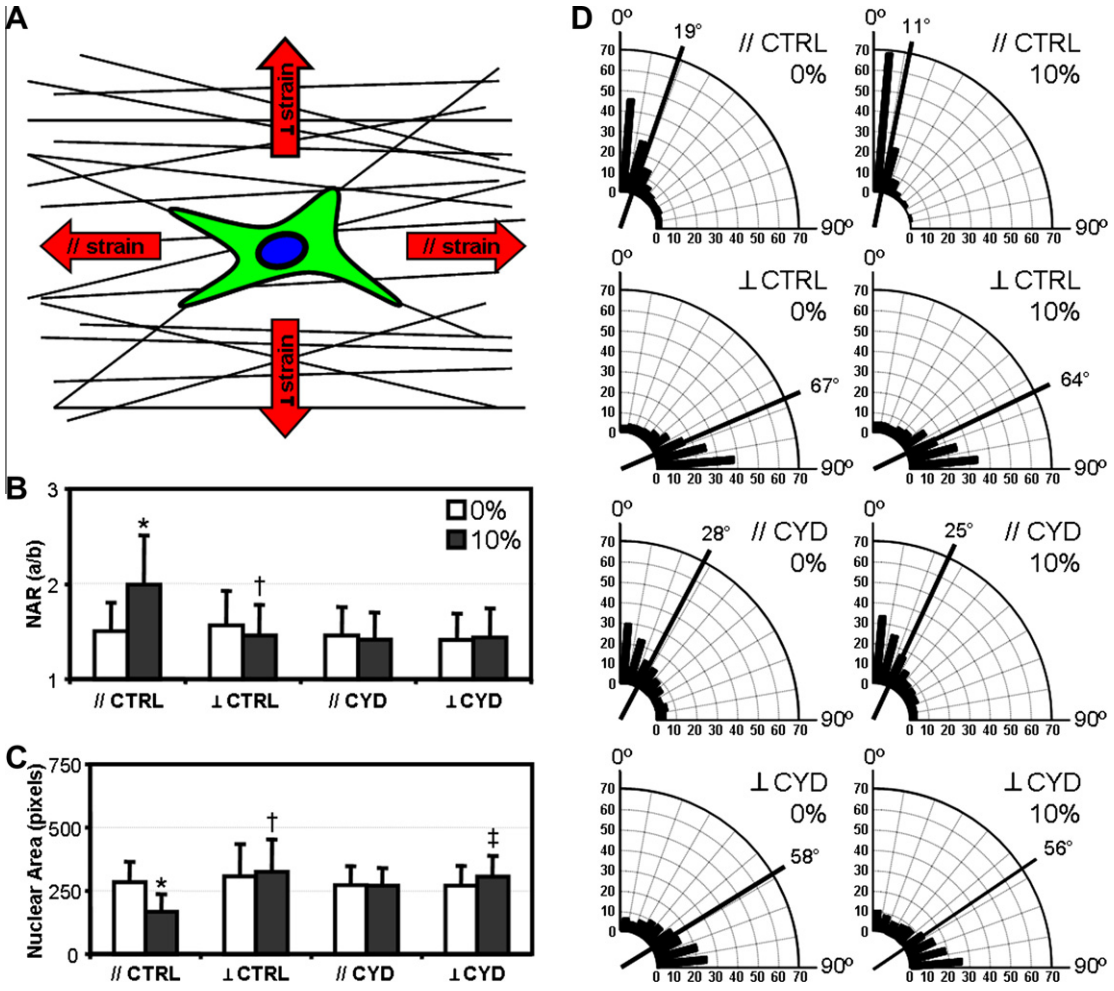

Fig. 7. Alterations in nuclear morphology are dependent on nanofiber stretch. (A) Schematic depicting strains applied parallel (//) and perpendicular (⊥) to the predominant fiber direction. Fibrochondrocyte seeded constructs were loaded in either direction in the presence or absence of CYD. (B) NAR, (C) nuclear area and (D) angular histograms were acquired from DAPI-stained images and normalized to pre-strain values ($n > 500$, $^{*}P < 0.05$ vs. 0% //CTRL, $^{\dagger}P < 0.05$ vs. 0% ⊥CTRL, $^{\ddagger}P < 0.05$ vs. ⊥CYD).

loading as a strategy for enhancing long-term extracellular matrix deposition or differentiation in engineered tissues if sustained nuclear deformation is required for these processes to occur.

Translation of scaffold deformation through the cell to nuclear deformation is mediated by the cytoskeletal network [31]. To determine which component of this network was operative in sensing topography and responding to applied deformation, selective disruption of actin, microtubule, and intermediate filament networks was carried out. Disruption of actin filaments blocked all NAR changes with stretch in the fiber or transverse directions, while disruption of microtubules and intermediate filaments had no effect on NAR with stretch. This finding suggests that the primary mediator of nuclear deformation on nanofibrous scaffolds is the actin network. Interestingly, blockade of both the microtubule and intermediate filament networks in the undeformed state led to a small but significant increase in NAR in MSCs. This may suggest that these two elements act to restrain the otherwise compressive action of the dense actin fibers that surround the nucleus and traverse the cell in the long axis. This is consistent with previous reports that the intermediate filament network is tightly coupled with the nucleus, determined by micromanipulation of cytoskeletal elements within a single cell [30]. Perturbations of the intermediate filament and microtubule network did not alter the nuclear morphology in fibrochondrocytes, again suggesting that the differentiated nucleus may be better able to resist deformation.

In the studies above 10% elongation of aligned scaffolds in the fiber direction caused an increase in NAR of ~30%, concomitant with decreases in nuclear area. Conversely, the same magnitude of strain applied transversely led to marginal changes in NAR and nuclear area in the opposite direction. This disparate behavior between 10% strain in the fiber parallel and perpendicular directions may be a consequence of scaffold mechanics [54]: loading in the fiber parallel direction induces large lateral contractions (large Poisson ratios), such that uniaxial extension along the fiber direction simultaneously extends the long axis of the nucleus and compresses the short axis. On the other hand, lateral contractions are very small under transverse extension, so that the cells are not subject to these compressive deformations. Indeed, under these conditions there is a small, but significant, decrease in NAR, suggesting that the nuclei of cells spread over multiple fibers may rebound as pre-stress from the actin cytoskeleton is partially relieved. This observation may also explain the differential expression patterns observed in MSCs on micro-grooved surfaces when stretched along and transverse to the groove (and cell) direction [27]. While future studies employing three-dimensional measurements via confocal imaging will be informative of changes in nuclear volume with deformation, the current findings suggest that substrate architecture alters the transmission of external forces inward, differentially altering nuclear shape, indicating a clear coupling of topographic and mechanical cues.

5. Conclusions

Taken together, these findings demonstrate that mechanical deformation of aligned nanofibrous scaffolds translates directly to cellular and sub-cellular changes in seeded MSCs and fibrochondrocytes. These alterations, particularly those of the nucleus, are time-dependent and mediated by the actin cytoskeleton. Furthermore, differences in nuclear morphology in response to mechanical load and presented topography support the idea of a more pliable nucleus in undifferentiated compared with differentiated cells. These data provide additional insight into potential biophysical mechanisms that may be optimized to improve fibrous tissue maturation through tailored mechanical loading regimens, as well as exploitable cues for defining and enforcing stem cell fate.

Acknowledgements

This work was funded in part by the Aircast Foundation, the Penn Center for Musculoskeletal Disorders (NIH AR050950), the National Institutes of Health (NIH EB02425 and AR056624), a Graduate Research Fellowship from the National Science Foundation (B.M.B.), and the Human Frontiers in Science Program. Support was additionally provided by the University Scholars program at the University of Pennsylvania (A.S.N.).

Appendix A. Figures with essential colour discrimination

Certain figures in this article, particularly Figs. 1, 2, 5 and 7 are difficult to interpret in black and white. The full colour images can be found in the on-line version, at doi: 10.1016/j.actbio.2010.08.007.

References

[1] Baksh D, Song L, Tuan RS. Adult mesenchymal stem cells: Characterization, differentiation, and application in cell and gene therapy. J Cell Mol Med 2004;8:301–16.
[2] Caplan AI. Mesenchymal stem cells. J Orthop Res 1991;9:641–50.
[3] Pittenger MF, Mackay AM, Beck SC, Jaiswal RK, Douglas R, Mosca JD, et al. Multilineage potential of adult human mesenchymal stem cells. Science 1999;284:143–7.
[4] Guilak F, Cohen DM, Estes BT, Gimble JM, Liedtke W, Chen CS. Control of stem cell fate by physical interactions with the extracellular matrix. Cell Stem Cell 2009;5:17–26.
[5] Discher DE, Mooney DJ, Zandstra PW. Growth factors, matrices, and forces combine and control stem cells. Science 2009;324:1673–7.
[6] Lee HJ, Yu C, Chansakul T, Hwang NS, Varghese S, Yu SM, et al. Enhanced chondrogenesis of mesenchymal stem cells in collagen mimetic peptide-mediated microenvironment. Tissue Eng Part A 2008;14:1843–51.
[7] Connelly JT, Garcia AJ, Levenston ME. Inhibition of in vitro chondrogenesis in RGD-modified three-dimensional alginate gels. Biomaterials 2007;28:1071–83.
[8] Dalby MJ, Gadegaard N, Curtis AS, Oreffo RO. Nanotopographical control of human osteoprogenitor differentiation. Curr Stem Cell Res Ther 2007;2:129–38.
[9] McBeath R, Pirone DM, Nelson CM, Bhadriraju K, Chen CS. Cell shape, cytoskeletal tension, and RhoA regulate stem cell lineage commitment. Dev Cell 2004;6:483–95.
[10] Mauck RL, Baker BM, Nerurkar NL, Burdick JA, Li WJ, Tuan RS, et al. Engineering on the straight and narrow: the mechanics of nanofibrous assemblies for fiber-reinforced tissue regeneration. Tissue Eng B Rev 2009;15:171–93.
[11] Li WJ, Tuli R, Huang X, Laquerriere P, Tuan RS. Multilineage differentiation of human mesenchymal stem cells in a three-dimensional nanofibrous scaffold. Biomaterials 2005;26:5158–66.
[12] Li WJ, Jiang YJ, Tuan RS. Chondrocyte phenotype in engineered fibrous matrix is regulated by fiber size. Tissue Eng 2006;12:1775–85.
[13] Ahmed I, Ponery AS, Nur EKA, Kamal J, Meshel AS, Sheetz MP, et al. Morphology, cytoskeletal organization, and myosin dynamics of mouse embryonic fibroblasts cultured on nanofibrillar surfaces. Mol Cell Biochem 2007;301:241–9.
[14] Nur EKA, Ahmed I, Kamal J, Schindler M, Meiners S. Three-dimensional nanofibrillar surfaces promote self-renewal in mouse embryonic stem cells. Stem cells 2006;24:426–33.
[15] Nur EKA, Ahmed I, Kamal J, Schindler M, Meiners S. Three dimensional nanofibrillar surfaces induce activation of Rac. Biochem Biophys Res Commun 2005;331:428–34.
[16] Li WJ, Mauck RL, Cooper JA, Yuan X, Tuan RS. Engineering controllable anisotropy in electrospun biodegradable nanofibrous scaffolds for musculoskeletal tissue engineering. J Biomech 2007;40:1686–93.
[17] Baker BM, Mauck RL. The effect of nanofiber alignment on the maturation of engineered meniscus constructs. Biomaterials 2007;28:1967–77.
[18] Nerurkar NL, Baker BM, Sen S, Wible EE, Elliott DM, Mauck RL. Nanofibrous biologic laminates replicate the form and function of the annulus fibrosus. Nat Mater 2009;8:986–92.
[19] Baker BM, Nathan AS, Gee AO, Mauck RL. The influence of an aligned nanofibrous topography on human mesenchymal stem cell fibrochondrogenesis. Biomaterials 2010;31:6190–200.
[20] Mouw JK, Connelly JT, Wilson CG, Michael KE, Levenston ME. Dynamic compression regulates the expression and synthesis of chondrocyte-specific matrix molecules in bone marrow stromal cells. Stem Cells 2007;25:655–63.
[21] Huang AH, Farrell MJ, Kim M, Mauck RL. Long-term dynamic loading improves the mechanical properties of chondrogenic mesenchymal stem cell-laden hydrogel. Eur Cell Mater 2010;19:72–85.

[22] Park JS, Chu JS, Cheng C, Chen F, Chen D, Li S. Differential effects of equiaxial and uniaxial strain on mesenchymal stem cells. Biotechnol Bioeng 2004;88:359–68.
[23] Simmons CA, Matlis S, Thornton AJ, Chen S, Wang CY, Mooney DJ. Cyclic strain enhances matrix mineralization by adult human mesenchymal stem cells via the extracellular signal-regulated kinase (ERK1/2) signaling pathway. J Biomech 2003;36:1087–96.
[24] Wang JH, Grood ES. The strain magnitude and contact guidance determine orientation response of fibroblasts to cyclic substrate strains. Connect Tissue Res 2000;41:29–36.
[25] Kaunas R, Nguyen P, Usami S, Chien S. Cooperative effects of Rho and mechanical stretch on stress fiber organization. Proc Natl Acad Sci USA 2005;102:15895–900.
[26] Wang JH, Jia F, Gilbert TW, Woo SL. Cell orientation determines the alignment of cell-produced collagenous matrix. J Biomech 2003;36:97–102.
[27] Kurpinski K, Chu J, Hashi C, Li S. Anisotropic mechanosensing by mesenchymal stem cells. Proc Natl Acad Sci USA 2006;103:16095–100.
[28] Wang N, Butler JP, Ingber DE. Mechanotransduction across the cell surface and through the cytoskeleton. Science 1993;260:1124–7.
[29] Chen CS, Ingber DE. Tensegrity and mechanoregulation: from skeleton to cytoskeleton. Osteoarthritis Cartilage 1999;7:81–94.
[30] Maniotis AJ, Chen CS, Ingber DE. Demonstration of mechanical connections between integrins, cytoskeletal filaments, and nucleoplasm that stabilize nuclear structure. Proc Natl Acad Sci USA 1997;94:849–54.
[31] Wang N, Tytell JD, Ingber DE. Mechanotransduction at a distance. Mechanically coupling the extracellular matrix with the nucleus. Nat Rev Mol Cell Biol 2009;10:75–82.
[32] Dahl KN, Ribeiro AJ, Lammerding J. Nuclear shape, mechanics, and mechanotransduction. Circ Res 2008;102:1307–18.
[33] Thomas CH, Collier JH, Sfeir CS, Healy KE. Engineering gene expression and protein synthesis by modulation of nuclear shape. Proc Natl Acad Sci USA 2002;99:1972–7.
[34] Knight MM, t Bravenboer J, Lee DA, van Osch GJ, Weinans H, Bader DL. Cell and nucleus deformation in compressed chondrocyte–alginate constructs: Temporal changes and calculation of cell modulus. Biochim Biophys Acta 2002;1570:1–8.
[35] Guilak F. Compression-induced changes in the shape and volume of the chondrocyte nucleus. J Biomech 1995;28:1529–41.
[36] Hoshiba T, Yamada T, Lu H, Kawazoe N, Tateishi T, Chen G. Nuclear deformation and expression change of cartilaginous genes during in vitro expansion of chondrocytes. Biochem Biophys Res Commun 2008;374:688–92.
[37] Zhang Z, Messana J, Hwang NS, Elisseeff JH. Reorganization of actin filaments enhances chondrogenic differentiation of cells derived from murine embryonic stem cells. Biochem Biophys Res Commun 2006;348:421–7.
[38] Buxboim A, Ivanovska IL, Discher DE. Matrix elasticity, cytoskeletal forces and physics of the nucleus: How deeply do cells 'feel' outside and in? J Cell Sci 2010;123:297–308.
[39] Pajerowski JD, Dahl KN, Zhong FL, Sammak PJ, Discher DE. Physical plasticity of the nucleus in stem cell differentiation. Proc Natl Acad Sci USA 2007;104:15619–24.
[40] Baker BM, Nathan AS, Huffman GR, Mauck RL. Tissue engineering with meniscus cells derived from surgical debris. Osteoarthritis Cartilage 2009;17:336–45.
[41] Mauck RL, Martinez-Diaz GJ, Yuan X, Tuan RS. Regional variation in meniscal fibrochondrocyte multi-lineage differentiation potential: Implications for meniscal repair. Anat Rec 2007;290:48–58.
[42] Mauck RL, Yuan X, Tuan RS. Chondrogenic differentiation and functional maturation of bovine mesenchymal stem cells in long-term agarose culture. Osteoarthritis Cartilage 2006;14:179–89.
[43] Trickey WR, Vail TP, Guilak F. The role of the cytoskeleton in the viscoelastic properties of human articular chondrocytes. J Orthop Res 2004;22:131–9.
[44] Connolly JA. Microtubules, microfilaments and the transport of acetylcholine receptors in embryonic myotubes. Exp Cell Res 1985;159:430–40.
[45] Nerurkar NL, Mauck RL, Elliott DM. ISSLS prize winner: Integrating theoretical and experimental methods for functional tissue engineering of the annulus fibrosus. Spine 2008;33:2691–701.
[46] Vargas DY, Raj A, Marras SA, Kramer FR, Tyagi S. Mechanism of mRNA transport in the nucleus. Proc Natl Acad Sci USA 2005;102:17008–13.
[47] Cremer T, Cremer M, Dietzel S, Muller S, Solovei I, Fakan S. Chromosome territories – a functional nuclear landscape. Curr Opin Cell Biol 2006;18:307–16.
[48] Baker BM, Shah RP, Mauck RL. Dynamic tensile loading improves the mechanical properties of MSC-laden aligned nanofibrous scaffolds. In: Proceedings of the ASME 2010 Summer Bioengineering Conference (SBC2009). Naples, FL: ASME; 2010. p. 19447.
[49] Yim EK, Darling EM, Kulangara K, Guilak F, Leong KW. Nanotopography-induced changes in focal adhesions, cytoskeletal organization, and mechanical properties of human mesenchymal stem cells. Biomaterials 2010;31:1299–306.
[50] Guilak F, Tedrow JR, Burgkart R. Viscoelastic properties of the cell nucleus. Biochem Biophys Res Commun 2000;269:781–6.
[51] Dahl KN, Kahn SM, Wilson KL, Discher DE. The nuclear envelope lamina network has elasticity and a compressibility limit suggestive of a molecular shock absorber. J Cell Sci 2004;117:4779–86.
[52] Stella JA, Liao J, Hong Y, David Merryman W, Wagner WR, Sacks MS. Tissue-to-cellular level deformation coupling in cell micro-integrated elastomeric scaffolds. Biomaterials 2008;29:3228–36.
[53] Putnam AJ, Cunningham JJ, Pillemer BB, Mooney DJ. External mechanical strain regulates membrane targeting of Rho GTPases by controlling microtubule assembly. Am J Physiol Cell Physiol 2003;284:C627–39.
[54] Nerurkar NL, Baker BM, Chen CY, Elliott DM, Mauck RL. Engineering of fiber-reinforced tissues with anisotropic biodegradable nanofibrous scaffolds. Conf Proc IEEE Eng Med Biol Soc 2006;1:787–90.